

Preparation and Characterization of Electrospun PCL/Silk Fibroin Scaffolds



This work is licensed under a Creative Commons Attribution 4.0 International License

E. Govorčin Bajsić,^a E. Zdraveva,^b T. Holjevac Grgurić,^c I. Slivac,^d M. Tominac Trcin,^e N. Mrkonjić,^a S. Kuzmić,^f T. Dolenc,^g I. Vrgoč Zimić,^g and B. Mijović^{b,*}

^aUniversity of Zagreb, Faculty of Chemical Engineering and Technology, Marulićev trg 19, 10000 Zagreb, Croatia

^bUniversity of Zagreb, Faculty of Textile Technology, Prilaz baruna Filipovića 28a, 10000 Zagreb, Croatia

^cUniversity of Zagreb, Faculty of Metallurgy, Aleja narodnih heroja 3, 44000 Sisak, Croatia

^dUniversity of Zagreb, Faculty of Food Technology and Biotechnology, Pierottijeva ul. 6, 10000 Zagreb, Croatia

^eThe Institute of Immunology, Rockefellerova 2, 10000 Zagreb, Croatia

^fForensic Science Centre “Ivan Vučetić”, Ilica 335, 10000 Zagreb, Croatia

^gSestre Milosrdnice University Hospital Center, Department of Transfusion and Regenerative Medicine, Draškovićeveva 19, Zagreb, Croatia

doi: <https://doi.org/10.15255/CABEQ.2020.1834>

Original scientific paper

Received: June 13, 2020

Accepted: March 29, 2021

Natural polymer-based scaffolds are generally considered as favourable matrices for the adhesion and growth of cells in tissue repair. One of the most popular materials in this respect is silk fibroin, known for its wide usage in biomedical applications. This work focuses on the development of electrospun scaffolds based on poly(ϵ -caprolactone) (PCL) and silk fibroin (SF) evaluated regarding the SF effect on their morphology, surface wetting ability, thermal properties, and HaCaT model cell line biocompatibility. The study revealed that the lowest PCL/SF concentration resulted in highest bead-like morphology formation, relatively thick fibers with the presence of random beads in the case of PCL, while uniform and thinner fibers in the case of increasing PCL/SF content scaffolds. The addition of SF reduced the degree of crystallinity in the PCL due to the less organized crystal structure, and decreased its thermal stability. Both SEM and MTT analyses showed cell presence on all scaffolds three days after cell seeding. Although SF improved PCL hydrophilicity, as shown quantitatively by the MTT assay for improved cytocompatibility properties, more structured electrospun PCL/SF scaffold strategies are required.

Keywords:

electrospinning, poly (ϵ -caprolactone), silk fibroin, scaffold, HaCaT cell line

Introduction

Regenerative medicine and tissue engineering are regarded as promising biomedical fields for the regeneration of damaged tissues or organs as an alternative to traditional transplantation. World public health is facing huge problems of tissue/organ donor scarcity or postoperative inflammatory tissue reactions, thus scaffold cell culturing has become of paramount importance among many research groups, and is expanding continuously.¹ The strategies for the development of biological substitutes

include: 1) cell isolation or cell substitutes, 2) tissues isolated substitutes or 3) cells grown on or within matrix scaffolding, thus to maintain, restore or improve the function of damaged tissues.² The aim of the introduction of a scaffolding material combined with stem cells and cells simulating growth factors, is to accelerate and improve the tissue healing process.³ A scaffold is supposed to be an artificial extracellular matrix composed of synthetic or natural polymers, bioceramics or hybrid materials, whether they are configured into fibrous-like, foam-like, sponge, woven, gradient or similar hierarchical architecture.^{4,5} Changes in structure and surface topography caused by fabrication

*Corresponding author: E-mail: budimir.mijovic@ttf.hr

processes may affect some of the properties of biomaterials, such as mechanical strength, cell adhesion, and degradation behaviour.

Both scaffold composition and structure are important in creating *in vivo*-like microenvironment that will mimic the natural cells surrounding and stimulate cell-specific responses to result in tissue repair.⁶ Tissue-cultured cells can sense scaffolds specific cues, including pores, grain size, and surface topography, which will finally determine the cells' fate pathways to differentiation. All the aforementioned cues affect cell adhesion, crawling, growth, and proliferation, as well as nutrient and metabolite transport, and protein adsorption.^{7,8} In regard to scaffold composition, generally a natural material is more favourable for cell scaffold interaction due to its biocompatibility and biodegradability. However, due to immunogenicity issues, fabricated materials or their combination with natural polymers would be a better choice. One much used natural polymer is that derived from the silk cocoon. It is known for its good mechanical properties, biocompatibility, ease of processability, and availability.^{9,10} Its applications include surgical threads,¹¹ blood vessels, skin and bone regeneration, drug transport,^{12–15} etc. On the other hand, poly(ϵ -caprolactone) (PCL) has been hugely investigated as a matrix material to natural polymers providing good support to system biodegradability, biocompatibility, and mechanical stability. The main disadvantages of PCL are its hydrophobicity, which is unfavourable for cell attachment and infiltration, and its slow degradation, which can last up to 3 or 4 years. Modification of its properties can be achieved by co-polymerization or blending with other polymers. Silk fibroin can be incorporated into poly(ϵ -caprolactone) (PCL) as reinforcement, and can significantly improve the mechanical properties of PCL, adding tuneable porosity and a durable framework to the scaffold. The added stiffness of PCL/silk scaffold composite can increase osteoblast attachment and differentiation in bone tissue engineering. Bone tissue engineering can be transplanted as grafts from other parts of the body or cadavers, but these strategies have many disadvantages.^{16–19} A better alternative to the current clinical treatment would be to construct a scaffold matrix with natural or synthetic polymers, polymer blends, or polymer–ceramic composites, which could limit the need for donor tissue, extended surgery, and risk of infection.¹⁶ SF are favourable for bone tissue engineering offering advantages such as biodegradability, biocompatibility, mechanical behavior, ease of processability, exceptional flexibility, and porosity.¹⁷ Silk fibroin has proved to be a biocompatible biomaterial, which supports cell attachment for bone regeneration. SF is capable of enhancing new bone formation. The degradation rate of silk-based

biomaterials can be tailored from months to years after implanting *in vivo*, based on processing procedures employed during material formation. Many *in vitro* and *in vivo* studies have shown that the degradability of SF porous biomaterials is related to the mode of processing and the corresponding content of β -sheet crystalline form. Finally, the thermal stability of silk biomaterials allows processing over a wide range of temperatures, up to about 250 °C, as evidenced by the ability to autoclave silk material systems without loss of functional integrity. Biodegradation behaviours of SF porous materials play an important role in regenerative biomedicine. In this study, a silk fibroin-based electrospun scaffold was developed to evaluate its effect on the response of HaCaT cell line, and opposite from the expected, it resulted in a less favourable effect of the silk fibroin on the adhered cells compared to the pure matrix synthetic (PCL) polymer. HaCaT cells are spontaneously immortalized keratinocytes from adult human skin, and have been proposed as a model cell line in much skin-related research *in vitro*. These cells are non-tumorigenic and monoclonal, adapted to long-term growth without feed-layer or supplemented growth factors; they exhibit normal morphogenesis and express all the major surface markers and functional activities of primary keratinocytes.^{20,21}

Experimental part

Materials

Polymers used in this study were polycaprolactone (PCL) $M_n = 80,000$ (Sigma Aldrich) and silk fibroin (SF) $M_w = 250,000$ (Huzhou Xintiansi Biotech Co, Ltd, China) in the form of a powder. Because SF is coated with sericin, degumming is very important. Sericins are a more hydrophilic protein, whose primary structure is richer in polar residues, but some of its fractions are not completely water soluble due to β -sheet portions. Silk fibroin used in this study was without sericin fractions. The removal of sericin is essential for the production of non-cytotoxic and non-allergic biomaterials for its clinical applications.

Solvents used in this study were glacial acetic acid and acetone (Ru-Ve). The electrical conductivity of the epoxy resin 3D printed collector was obtained by a graphite spray coating (CRC Industries Europe).

Electrospinning of the PCL/Silk fibroin solutions

Homogeneous solutions were prepared by dissolving the PCL in a mixture of glacial acetic acid and acetone, with the volume ratio of 8:2, and adding the SF with constant stirring. The concentra-

tions of the PCL were 10, 12, 14, 16, and 18 wt%, while the SF was 50 wt% of the mass of the PCL.

Electrospun PCL/SF scaffolds were prepared on a standard electrospinning device NT-ESS-300, NTSEE Co. Ltd., South Korea, with a modified collector.²² The processing conditions were electrical voltage of 17–21 kV, needle tip to collector distance of 18 cm, and volume flow rate of 1 mL h⁻¹.

Characterization

SEM analysis

The morphology of the pure PCL, SF, and PCL/SF electrospun scaffolds was observed using Tescan VEGA, Mira 3 scanning electron microscope (SEM) with a previous gold coating.

FTIR-ATR spectroscopy

The characteristic absorption peaks of the PCL and PCL/SF electrospun scaffolds were determined by ATR-Fourier transform infrared (ATR-FTIR) spectroscopy on a PerkinElmer Spectrum One FTIR spectrometer. All spectra were recorded at room temperature in the range of 650–4000 cm⁻¹ with a resolution of 4 cm⁻¹.

Water contact angle measurement

The wetting ability of the electrospun PCL and PCL/SF scaffolds was determined by the contact angle method on DataPhysics OCA 20 Instruments GmbH device. The water drop volume was between 1 to 5 µL, and each water drop angle was measured after 20 seconds, while the samples were measured in triplicate.

Differential scanning calorimetry (DSC)

Thermal analysis of the electrospun PCL and PCL/SF scaffolds was performed on a DSC instrument Mettler Toledo DSC 822e (Mettler Toledo, Greifensee, Switzerland). Two heating-cooling cycles were performed by first cooling the sample from 25 °C to -100 °C, and then heating from -100 °C to 80 °C at a heating rate of 10 °C min⁻¹ in inert atmosphere. The sample weight was 5 mg, and the cooling was done under liquid nitrogen. The glass transition (T_g), melting temperature (T_m), and crystallization temperature (T_c) were determined from the second heating/cooling cycle. The melting enthalpies from the second heating cycle were used to calculate the degree of crystallinity (χ_c), according to equation 1:

$$\chi_c (\%) = \frac{\Delta H_m^o}{\Delta H_m^{100}} \cdot 100 \quad (1)$$

where: ΔH_m^o is the fusion enthalpy (J g⁻¹) determined by the DSC measurement, while ΔH_m^{100} is the heat fusion of 100 % crystalline PCL (142 J g⁻¹).²³

Thermogravimetric analysis (TGA)

The thermal stability of the electrospun scaffolds was determined by TGA analyser, Q500 TA Instruments. Samples of approximately 10 mg were heated from 25 to 700 °C at a heating rate of 10 °C min⁻¹ in a nitrogen atmosphere (60 mL min⁻¹).

HaCaT cell culture

The HaCaT cells inoculum was prepared in a Petri dish with DMEM and 10 % fetal bovine serum, incubated at 37 °C in humidified CO₂ incubator, while the scaffolds were cut to fit a 24-well plate (16 mm diameter). Sterilization of the scaffolds was performed by soaking in 70 % ethanol and exposure to UV light for 30 min, followed by three consecutive washing steps in PBS and culture media. Before the scaffold seeding, the cells were densely concentrated at 100.000 cells in 200 mL of media. This cell suspension was added in a drop-wise manner onto electrospun discs. The applied high cell density was chosen because it gives satisfactory cell confluence 6 and 72 hours after seeding, according to our earlier work.²⁴ Furthermore, since the process of cell seeding and adhesion on new surfaces is not a very efficient process, it is always better to add cells in slight excess. Three days after seeding, six discs/scaffolds were taken for standard 3-(4, 5-dimethylthiazol-2-yl)-2, 5-diphenyltetrazolium bromide (MTT) assay. The assay served for visual inspection of the cell-colonised scaffolds after they had turned purple due to the presence of viable cells. A spectrophotometer was used to obtain the absorbance values of the produced formazan dissolved in DMSO (wavelength 570 nm). The unseeded scaffolds were used as the control samples. They had undergone the same media incubation and staining treatment as the cell seeded scaffolds. Due to reduced manageability of the cell seeding procedure, all the experiments with HaCaT cells were performed twice in sextuplicate.

Results and discussion

Morphology of electrospun scaffolds

Generally, the morphological structure of the electrospun scaffolds depends on the solution parameters (viscosity, concentration, electrical conductivity, surface tension), and parameters of the electrospinning process (electric field, flow rate, needle diameter, and its distance from the collector). The SEM micrograph of the pure PCL scaffold (Fig. 1a) presents the formation of relatively thick fibers with random bead-morphology, but with mostly micellar-like defects. More uniform morphology, with finer fibers and reduced beads was obtained for the

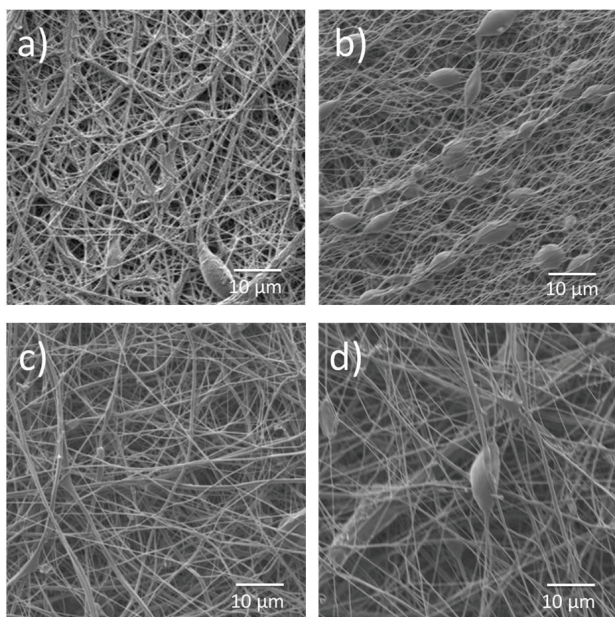


Fig. 1 – SEM micrographs of the PCL/silk fibroin scaffolds: a) PCL b) 10 % PCL/SF, c) 14 % PCL/SF and d) 18 % PCL/SF

electrospun 14 % PCL/SF and 18 % PCL/SF scaffolds (Fig. 1c, d). The lowest PCL/SF concentration showed bead-like structure throughout the fibers length. The observed changes in the fibers morphology generally resulted from the change in solution viscosity and surface tension caused by the addition of the SF, which sometimes needs modification of the initial electrical voltage set, thus finally affecting fiber diameter. Diezel *et al.*²⁵ have shown that the surface tension and viscosity of the solution play an important role in determining the range of the concentrations suitable for the formation of continuous fibers. Thus, as silk fibroin concentration increases, the fiber morphology changes from micellar-like structures to more uniform fibers, while at higher concentrations, the PCL fibers become thinner.

Other observations reported molecular weight of the components as the key factor controlling possible phase separation. Wei *et al.*²⁶ have shown that the morphology of phase-separated nanofibers depends on the relative ratio of the two polymers with different molecular weights.

Nanofibers consisting of a higher concentration of higher molecular weight polymer have a co-continuous structure, whereas in the case of a higher concentration of lower molecular weight polymer, the phase morphology of the nanofibers changes from co-continuous to a core-sheath structure. Silk fibroin is a polypeptide with high molecular weight consisting of heavy (350 kDa) and light (25 kDa) chains compared to PCL (90 kDa). Therefore, when the content of SF increases, it is expected that there

will be a change in the nanofiber morphology from a typical core-sheath structure to a co-continuous structure.²⁷ SF molecules with light (25 kDa) chains will be present on the surface of the PCL/SF fiber carrier due to their greater diffusion capacity than that of PCL.

FTIR-ATR characterization of the electrospun scaffolds

The FTIR-ATR technique was performed to confirm the incorporation of SF in the PCL matrix and its interaction with PCL matrix. The spectra of the SF, electrospun PCL, and PCL/SF scaffolds are presented in Fig. 2. The pure electrospun PCL shows the characteristic absorption peaks at 2944 and 2865 cm^{-1} , which are related to the asymmetrical and symmetrical stretching of the CH_2 groups, respectively. The most intense peak at 1720 cm^{-1} is related to the carbonyl ($\text{C}=\text{O}$) stretching in the amorphous phase.²⁸ The absorption peaks at 1470 and 1365 cm^{-1} are due to the $-\text{CH}$ bending of $-\text{CH}_3$ (symmetric) and OH in-plane bending vibrations, respectively. According to Coleman and Zarian, the peak at 1292 cm^{-1} is assigned to the backbone $\text{C}-\text{C}$ and $\text{C}-\text{O}$ stretching in the crystalline phase of the PCL.²⁹ The absorption peak observed at 1238 cm^{-1} was due to the $\text{C}-\text{O}-\text{C}$ asymmetric bond. The absorption band at 1165 cm^{-1} is related to the axial deformation of the $\text{C}-\text{C}(=\text{O})-\text{O}$, while the absorption band at 731 cm^{-1} is related to the $-(\text{CH}_2)-$ stretching vibration.³⁰ The FTIR-ATR spectra of the SF shows the characteristic absorption peak at 1619 cm^{-1} for the peptide backbone of amide I ($\text{C}=\text{O}$ stretching). The amide I vibration directly depends on the secondary structure of the silk fibroin protein backbone, and is most commonly used for the quantitative analysis of different secondary structures.³¹ The absorption peak at 1516 cm^{-1} corresponds to amide II (secondary $\text{N}-\text{H}$ bending vibration) due to the β -sheet structure,³² while the absorption peak at 1238 cm^{-1} is related to amide III ($\text{C}-\text{N}$ and $\text{N}-\text{H}$ stretching).³³ The new bands are observed at 1628 and 1521 cm^{-1} in 16 % PCL/SF and 18 % PCL/SF electrospun scaffolds. Characteristic, very strong $\text{C}=\text{O}$ stretching peak for PCL is also present at 1722 cm^{-1} in pure PCL and PCL/SF electrospun scaffolds. The presence of SF amide bands along with PCL characteristic bands confirms the incorporation of SF in PCL matrix in electrospun scaffolds. These results are also in good agreement with the literature data.^{34,35}

Electrospun scaffold hydrophilicity

Water-contact angle measurements are important as they provide information concerning the interaction between the material's surface and the wa-

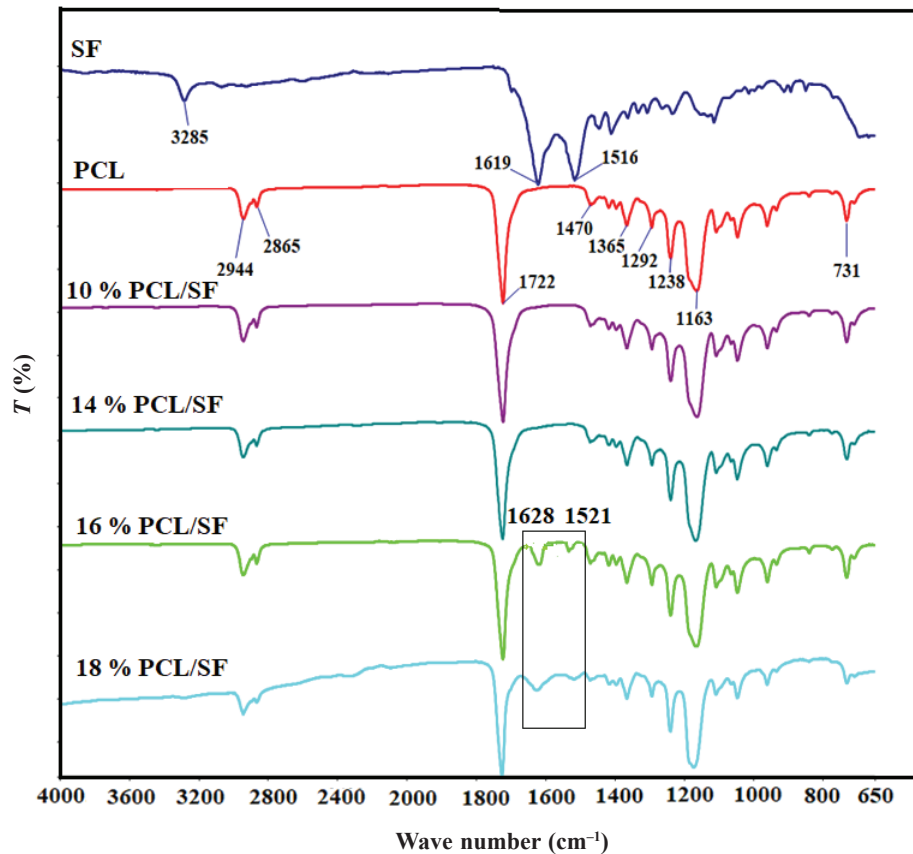


Fig. 2 – FTIR-ATR spectra of SF, electrospun PCL, and PCL/SF scaffolds

ter drop. In this work, the effect of the silk fibroin on PCL hydrophilicity was obtained through water-contact angle measurement on the surface of the PCL/SF scaffolds. Generally, PCL restricts any cellular interactions, due to its hydrophobic nature and absence of functional groups that enable cell growth and proliferation. Therefore, the surface of tissue engineered PCL scaffolds needs to be modified in order to enhance their cellular compatibility. The results of the measured water-contact angles and the appearance of the water drop on the surface of the scaffolds are given in Fig. 3 and Table 1. Contact angle for pure PCL electrospun scaffold was determined to be $125.8 \pm 5.6^\circ$ owing to the hydrophobic nature of PCL. From the results (Table 1), we can see that contact angle values for PCL/SF electrospun scaffolds decreased from $105.2 \pm 3.1^\circ$ to $46.5 \pm 4.3^\circ$. As expected, the results suggested that the high hydrophobicity of the pure electrospun PCL (water contact angle of $125.8 \pm 5.6^\circ$) was reduced by the addition of the silk fibroin. The hydrophilic groups in SF are amine, hydroxyl, and carboxyl groups.³⁶ Therefore, the addition of SF could improve the hydrophilicity of the PCL/SF electrospun scaffolds surfaces.

According to contact angle results (Table 1), it is clear that, with higher concentration of PCL in the electrospun PCL/SF scaffolds, a lower reduction

in water contact angle was noticed compared to pure PCL. Thus, the 18 % PCL/SF showed an angle of 105.2° , while all other PCL/SF scaffolds showed high hydrophilicity below 50° with less significant differences in the angle reduction. The wettability of the scaffolds resulted from the hydrophilic amide ($-\text{CONH}$) and hydroxyl ($-\text{OH}$) groups of the silk fibroin, as well as from the capillary effect generated by hydrophilic SF incorporation, and due to the presence of micro-/nano-pores on the electrospun surface. The introduction of surface hydrophilic groups of SF on the PCL surface led to an increase in surface free energy.

Table 1 – Water contact angle measured on the surface of the electrospun scaffolds

Electrospun scaffold	$\theta/^\circ$
18 % PCL	125.8 ± 5.6
10 % PCL/SF	46.5 ± 4.3
12 % PCL/SF	47.8 ± 3.0
14 % PCL/SF	38.8 ± 2.7
16 % PCL/SF	48.5 ± 5.5
18 % PCL/SF	105.2 ± 3.1

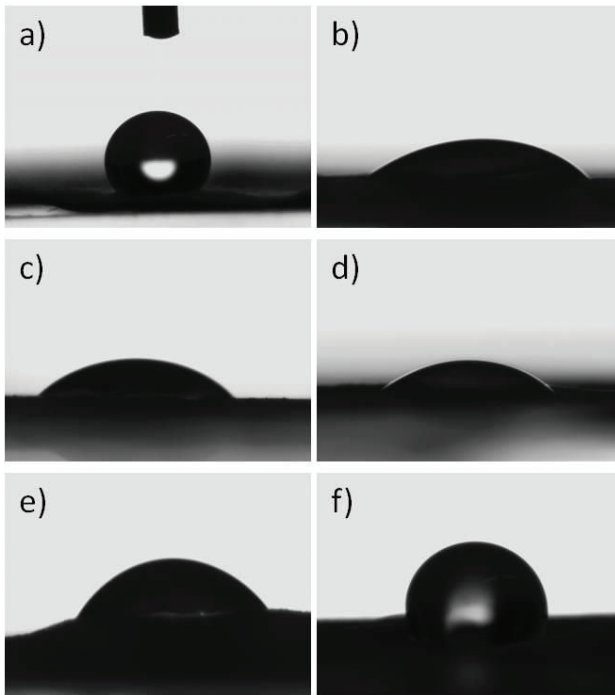


Fig. 3 – Water drops on the surface of the electrospun scaffolds: a) 18 % PCL, b) 10 % PCL/SF, c) 12 % PCL/SF, d) 14 % PCL/SF, e) 16 % PCL/SF, and f) 18 % PCL/SF

Generally, tissue cells prefer mild wetting surfaces, thus an optimal content combination of the two polymers.

Thermal properties of the electrospun scaffolds

DSC measurements were conducted to study the effect of SF on the thermal properties of the PCL/SF electrospun scaffolds. The thermal properties values after the second heating cycle include the glass transition temperature T_g , melting temperature T_m , crystallization temperature T_c , melting enthalpy ΔH_m , and degree of crystallinity χ_c , of the electrospun PCL and PCL/SF scaffolds (Table 2). The DSC heating curve of the SF, Fig. 4, is characterized by the endotherm at 68 °C due to moisture evaporation, the T_g of its amorphous phase at 109 °C, and the three higher temperature peaks.

The appearance of the endothermic peak at 128 °C is related to the silk I crystals or the random coil structure.³⁷ The endothermic peak at 247 °C is related to the melting temperature of the β -plates nanocrystals (with less ordered structure) in the silk II structure.³⁷ A broad endotherm peak with an onset at 280 °C can be related to the thermal decomposition of a well-organized crystalline SF structure.³⁸ Figs. 5a and b, show the DSC curves of the electrospun PCL and PCL/SF scaffolds during the heating and cooling cycle, respectively. The electrospun PCL scaffold, during heating, shows the glass transition temperature and melting temperature related to the crystalline phase at -63.4 °C and 58.2 °C, respectively. The exothermic peak at 27.6 °C relates to the crystallization of the PCL crystalline phase. These values are in agreement with PCL literature data.³⁹

The T_g of the pure PCL scaffold (at -63.4 °C) shifted to lower temperature with the addition of the silk fibroin. This decrease in the T_g may be due to increased degree of chain mobility in the PCL. The T_m of the pure PCL scaffold observed at 58.2 °C shifted to higher temperature in the case of the 12 % PCL/SF and 18 % PCL/SF electrospun scaffolds.

This behaviour might be due to the higher ordered crystalline structure in these electrospun scaffolds. The crystallization temperature of the PCL/SF electrospun scaffolds had slightly shifted to a higher temperature with the incorporation of the SF. The addition of the SF also resulted in decrease of the degree of crystallinity compared to the pure PCL scaffold.

Thermal degradation of the electrospun scaffolds

To understand blend scaffolds' thermal stability, the thermal degradation behaviour was firstly observed for the pure powder SF, Fig. 6, having three steps of degradation. In the first step, the weight loss (50 to 100 °C) was due to moisture evaporation, which was followed by a second large weight loss in the temperature range from 170 to 260 °C, corresponding to the evaporation of other

Table 2 – Transition temperatures and degree of crystallinity of the electrospun scaffolds

Electrospun scaffolds	T_g /°C	T_m /°C	T_c /°C	ΔH_m /J g ⁻¹	χ_c /%
PCL	-63.4	58.2	27.6	58.97	41.5
10 % PCL/SF	-63.9	57.1	31.0	56.11	39.5
12 % PCL/SF	-65.7	56.8	30.1	63.05	44.4
14 % PCL/SF	-63.7	55.6	27.0	55.34	39.0
16 % PCL/SF	-64.0	60.0	28.9	55.92	39.4
18 % PCL/SF	-63.1	59.2	28.7	50.60	35.6

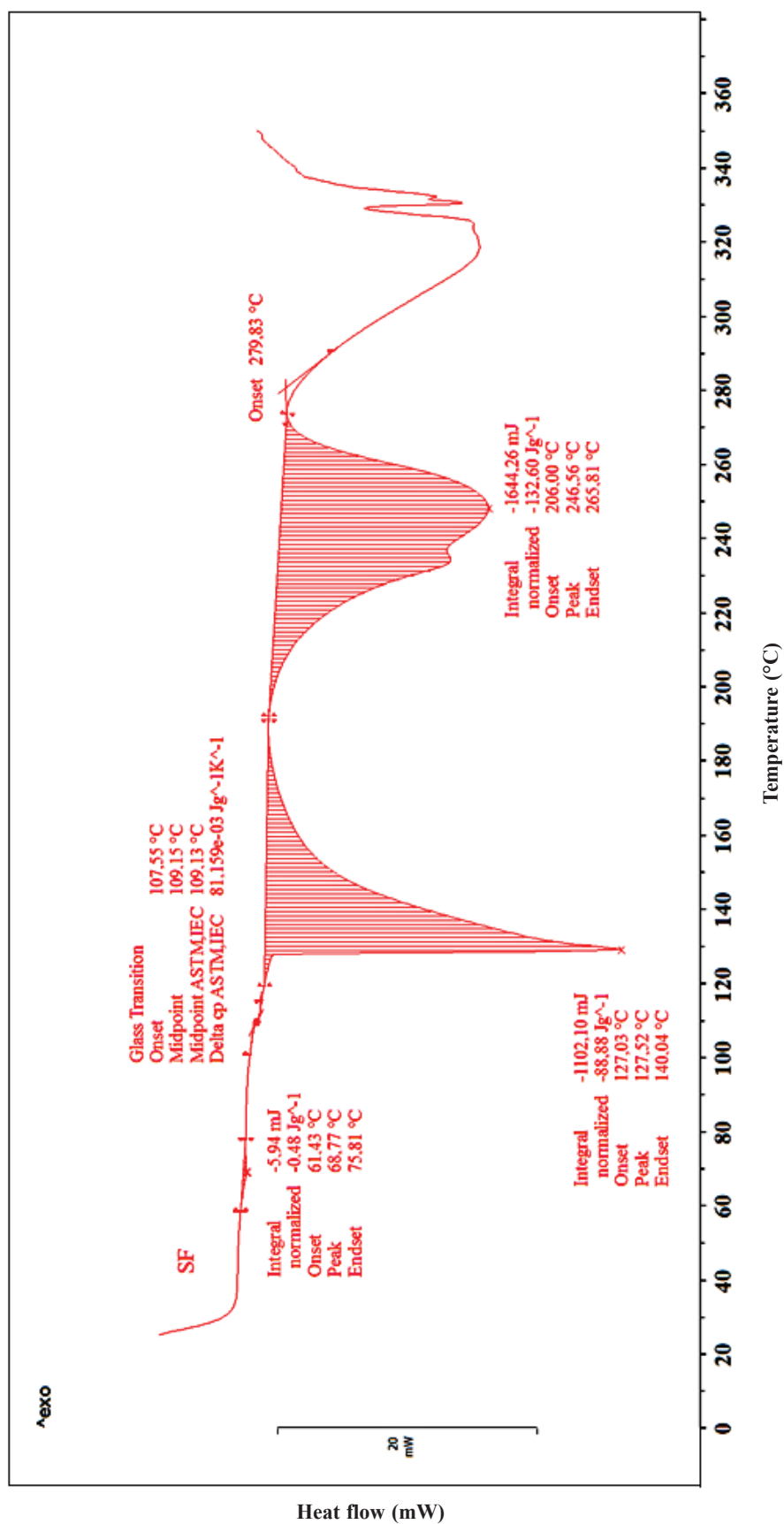


Fig. 4 – DSC curves of silk fibroin powder during heating

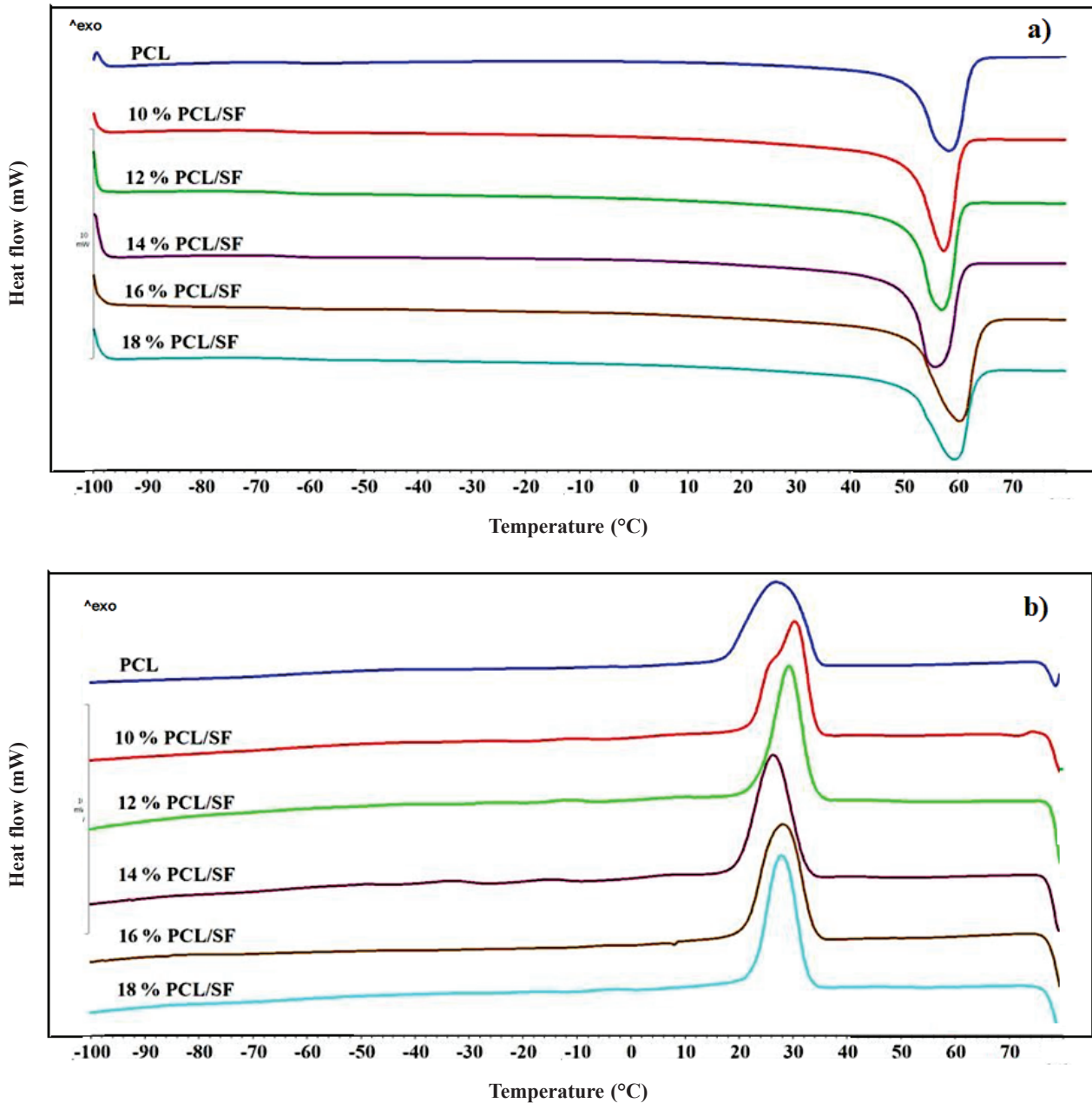


Fig. 5 – DSC curves of the electrospun PCL and PCL/SF scaffolds during second (a) heating, and (b) cooling cycle

volatile components. The third weight loss was associated with the degradation of the side chain groups of the amino acid residues and the cleavage of the peptide bonds.⁴⁰ Thermal degradation of silk proteins occurs primarily via end-group initiated depolymerization. The residual carbon weight was of 33.27%. The DTG and TG curves of the electrospun PCL and PCL/SF scaffolds are given in Figs. 7 and 8, respectively, while the temperature of 5% weight loss ($T_{5\%}$) and the maximum thermal degradation temperature (T_{max}) are summarized in Table 3.

The electrospun PCL shows a single degradation step, while the electrospun PCL/SF scaffolds show three steps of degradation. The electrospun

PCL started to decompose at 340.9 °C,⁴¹ and experienced a maximum weight loss at the temperature of 408.4 °C, while the electrospun PCL/SF scaffolds, except for the 12% PCL/SF and 14% PCL/SF, had $T_{5\%}$ lower than 300 °C. The first, second, and third degradation step of the electrospun PCL/SF scaffolds occurred at 100–150 °C, 150–250 °C and 250 to 350 °C, respectively. These were associated with the presence of the SF, while the last stage of degradation, above 350 °C, was due to the decomposition of the pure PCL. The T_{max} values obtained from 321 to 336 °C and 403 to 413 °C depend on the PCL content. When the PCL content increased, the thermal stability of the electrospun PCL/SF scaffold

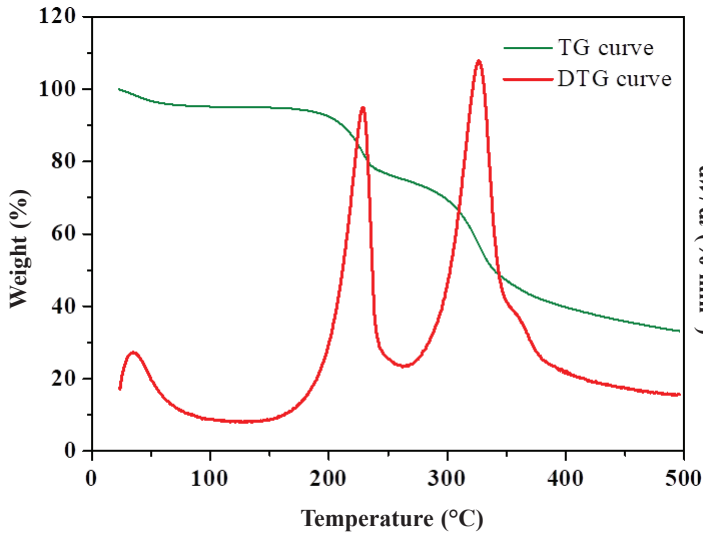


Fig. 6 – TG curves of the silk fibroin

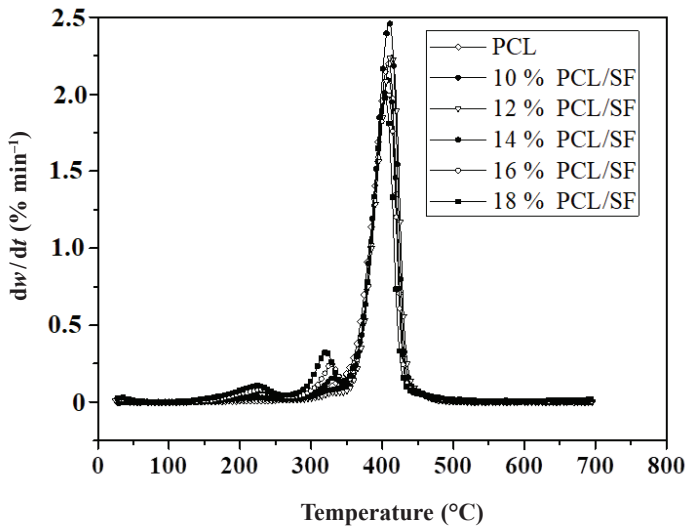


Fig. 7 – DTG curves of the electrospun PCL and PCL/SF scaffolds

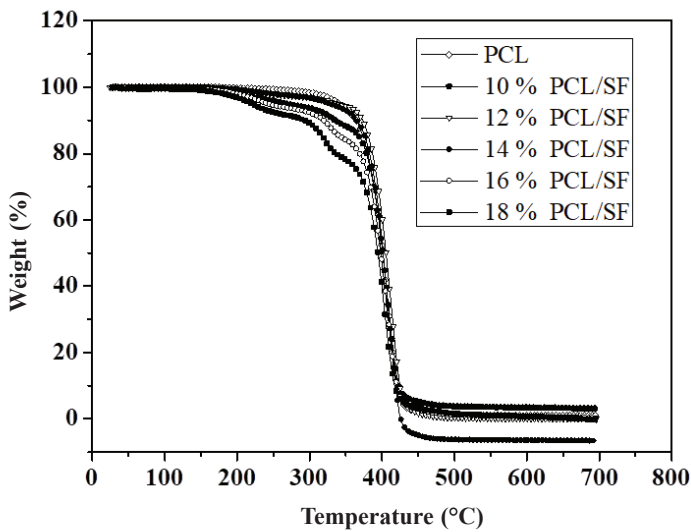


Fig. 8 – TG curves of the electrospun PCL and PCL/SF scaffolds

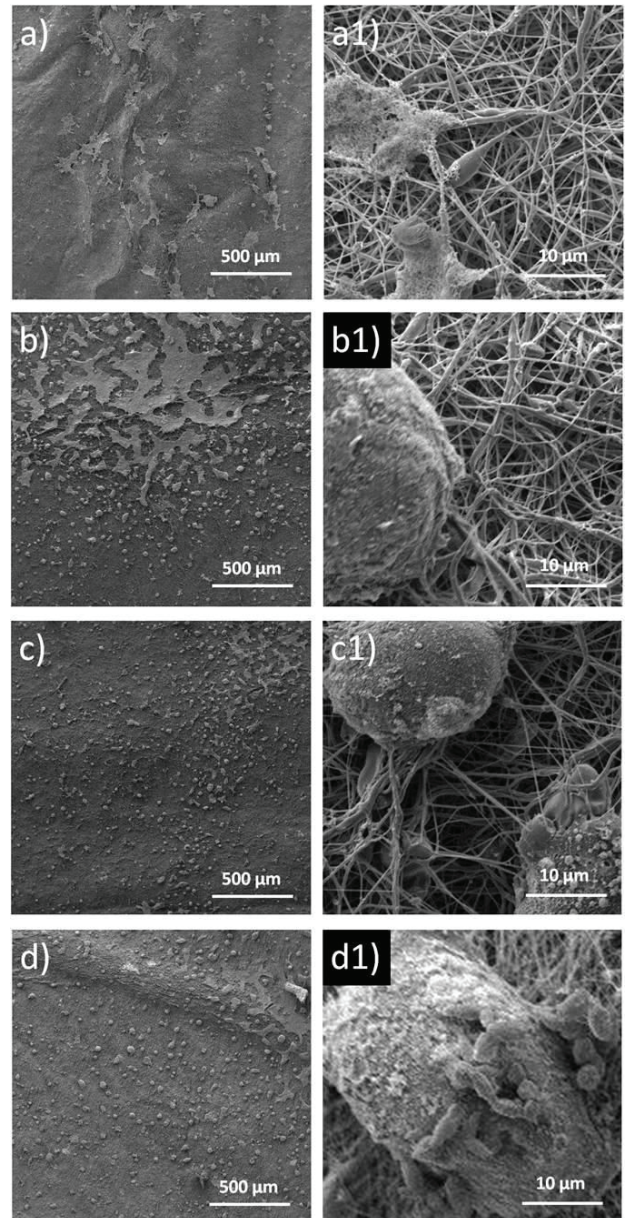


Fig. 9 – SEM images of the electrospun scaffolds cultured with HaCaT cells 72 hours after cell seeding, a/a1) PCL, b/b1) 10 % PCL/SF, c/c1) 14 % PCL/SF and d/d1) 18 % PCL/SF

Table 3 – Results of TG analysis for the pure electrospun PCL and electrospun PCL/SF scaffolds

Electrospun scaffolds	$T_{5\%}/$ °C	$T_f/$ °C	$T_{max,1}/$ °C	$T_{max,2}/$ °C	$T_{max,3}/$ °C
PCL 18 %	340.9	425.5	/	/	408.4
10 % PCL/SF	267.4	424.4	232.8	332.1	408.4
12 % PCL/SF	339.2	430.3	200.7	335.8	412.9
14 % PCL/SF	329.2	426.2	224.7	325.7	410.0
16 % PCL/SF	241.6	424.5	230.4	327.8	407.5
18 % PCL/SF	220.1	418.7	224.5	320.9	403.4

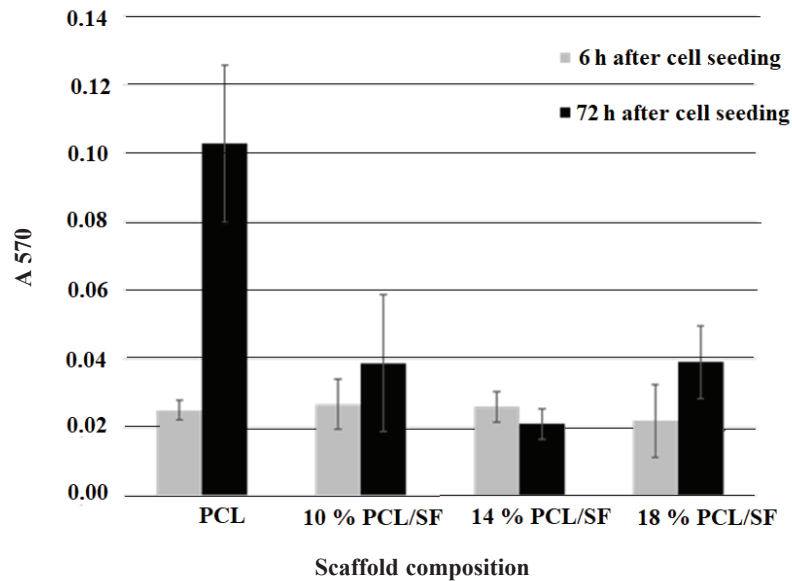


Fig. 10 – Formazan absorbance (A_{570}) as indicator of HaCaT cell confluence on the electrospun PCL/SF scaffolds. During MTT assay, viable cells growing on the scaffolds produce formazan, which is a purple metabolic derivative of tetrazolium salt. Scaffold samples without cells were used as the blank.

folds decreased compared to the pure electrospun PCL. At the same time, the intensity of the SF degradation peak increased. This change was due to the blending and incorporation of SF into the PCL matrix.

Evaluation of HaCaT cells adhesion on the electrospun scaffolds surface

The presence of HaCaT cells on the PCL/SF scaffolds was evaluated by SEM, as well as by cell MTT assay. Fig. 9 shows the microscopy images of HaCaT cells attached on the PCL and PCL/SF scaffolds 72 hours after cell seeding. With the applied magnification the difference in cell density on scaffold surface cannot be clearly estimated. However, it confirms at least that the cells are successfully attached and spread over all the scaffolds. To compare the efficacy of cell adhesion on four different surfaces, the seeded scaffolds were treated with MTT six hours after cell inoculation. The grey bars in Fig. 10 show that the viable cells are present in similar quantity on all tested scaffolds, indicating that the chosen composition blends support cell adhesion. To further estimate the cytocompatibility of the scaffolds, the cell proliferation was carried out 72 hours after seeding using the same MTT technique. The assessment clearly showed that the cells had preference for one of the four tested scaffolds. Expectedly, the highest formazan absorbance was found in the most colonised (i.e. the most purple stained) samples, but these were the scaffolds made of pure PCL (Fig. 10, black bars).

This was contrary to our anticipation that the hydrophilic nature of silk fibroin could contribute

favourably to cell adhesion. In contrast, three electrospun PCL/SF scaffolds did not significantly differ in their performance, which suggested that the SF content in the electrospun scaffolds had a decreasing effect on cell adhesion and proliferation. It is known that HaCaT cells, since originating from adult human skin, accommodate rather slowly to novel surfaces,⁴² which certainly made an impact on our results and suggested a more profound study of their adhesion and growth properties. Moreover, it is well known that pure SF exhibits poor attachment and proliferation for some cell types, such as neuronal cells, certain mesenchymal stem cells, and bone cells, so it is primarily used for improvement of mechanical strength and biodegradability in various blends.^{43,44} Finding appropriate SF portion in polymer blends should be a crucial preliminary step of any potential cell scaffold investigations. Our results indicate that PCL-based blends, where approximately one third of their composition is SF, may not be suitable for HaCaT cell growth. Therefore, a systematic blending of the two polymers with great reputation in biomedicine, will be our future goal.

Conclusion

This work focuses on the evaluation of the properties of electrospun PCL/SF scaffolds concerning their composition effects, and final HaCaT cell support function. The morphology of the fibrous scaffolds was influenced by the weight content of PCL to SF due to the change in solution viscosity and surface tension, thus resulting in bead-like fibers to uniform structures in the case of lower to

higher PCL/SF concentration, respectively. In respect to surface wettability, all PCL/SF scaffolds showed greater hydrophilicity compared to the pure electrospun PCL scaffold, although higher PCL concentration led to lower water-contact angle reduction. The addition of the SF into the pure PCL also affected its thermal properties. Thus, the PCL/SF scaffolds showed reduced both degree of crystallinity and thermal stability. Unexpectedly, the highest cell density and the best cell distribution was found on scaffolds made of pure PCL. Despite modified physical properties, the electrospun PCL/SF scaffolds failed the cell proliferation test. It seems that for improved cytocompatibility properties, more structured electrospun PCL/SF scaffold strategies are required.

ACKNOWLEDGEMENT

This work has been fully supported by Croatian Science Foundation under the project IP-2016-06-6878, Custom Tailored Fibrous Scaffold Prototype for Tissue Cells Culture via Combined Electrospinning, COMBOELECTROSPUN.

CONFLICT OF INTEREST

The authors declare that there is no conflict of interest.

References

- Pina, S., Ribeiro, V. P., Marques, C. F., Maia, F. R., Silva, T. H., Reis, R. L., Oliveira, J. M., Scaffolding strategies for tissue engineering and regenerative medicine applications, *Materials* **12** (2019) 1824. doi: <https://doi.org/10.3390/ma12111824>
- Langer, R., Vacanti, J., Tissue engineering, *Science* **May 14** (1993) 920. doi: <https://doi.org/10.1126/science.8493529>
- Dzobo, K., Thomford, N. E., Senthebane, D. A., Shipanga, H., Rowe, A., Dandara, C., Pillay, M., Motaung, K. S. C. M., Advances in regenerative medicine and tissue engineering: Innovation and transformation of medicine, *Stem Cells Int.* **2018** (2018) 24. doi: <https://doi.org/10.1155/2018/2495848>
- Jun, I., Han, H.-S., Edwards, J. R., Jeon, H., Electrospun fibrous scaffolds for tissue engineering: Viewpoints on architecture and fabrication, *Int. J. Mol. Sci.* **19** (2018) 745. doi: <https://doi.org/10.3390/ijms19030745>
- Eltom, A., Zhong, G., Muhammad, A., Scaffold techniques and designs in tissue engineering functions and purposes: A review, *Adv. Mater. Sci. Eng.* **2019** (2019) 13. doi: <https://doi.org/10.1155/2019/3429527>
- Karp, J. M., Dalton, P. D., Shoichet, M. S., Scaffolds for tissue engineering, *MRS Bull.* **28** (2003) 301. doi: <https://doi.org/10.1557/mrs2003.85>
- Chen, X., Fan, H., Deng, X., Wu, L., Yi, T., Gu, L., Zhou, C., Fan, Y., Zhang, X., Scaffold structural microenvironmental cues to guide tissue regeneration in bone tissue applications, *Nanomaterials* **8** (2018) 960. doi: <https://doi.org/10.3390/nano8110960>
- Skoog, S. A., Kumar, G., Narayan, R. J., Goering, P. L., Biological responses to immobilized microscale and nanoscale surface topographies, *Pharmacol. Therapeut.* **182** (2018) 33. doi: <https://doi.org/10.1016/j.pharmthera.2017.07.009>
- Kundu, B., Rajkhowa, R., Kundu, S. C., Wang, X., Silk fibroin biomaterials for tissue regenerations, *Adv. Drug Deliv. Rev.* **65** (2013) 457. doi: <https://doi.org/10.1016/j.addr.2012.09.043>
- Melke, J., Midha, S., Ghosh, S., Ito, K., Hofmann, S., Silk fibroin as biomaterial for bone tissue engineering, *Acta Biomater.* **31** (2016) 1. doi: <https://doi.org/10.1016/j.actbio.2015.09.005>
- Omenetto, F. G., Kaplan, D. L., New opportunities for an ancient material, *Science* **329** (2010) 528. doi: <https://doi.org/10.1126/science.1188936>
- Zhao, Z., Li, Y., Xie, M.-B., Silk fibroin-based nanoparticles for drug delivery, *Int. J. Mol. Sci.* **16** (2015) 4880. doi: <https://doi.org/10.3390/ijms16034880>
- Nakazawa, Y., Sato, M., Takahashi, R., Aytemiz, D., Takabayashi, C., Tamura, T., Enomoto, S., Sata, M., Asakura, T., Development of small-diameter vascular grafts based on silk fibroin fibers from *Bombyx mori* for vascular regeneration, *J. Biomater. Sci. Polym. Ed.* **22** (2011) 195. doi: <https://doi.org/10.1163/092050609X12586381656530>
- Roh, D.-H., Kang, S.-Y., Kim, J.-Y., Kwon, Y.-B., Kweon, H. Y., Lee, K.-G., Park, Y.-H., Baek, R.-M., Heo, C.-Y., Choe, J., Wound healing effect of silk fibroin/alginate-blended sponge in full thickness skin defect of rat, *J. Mater. Sci. Mater. Med.* **17** (2006) 547. doi: <https://doi.org/10.1007/s10856-006-8938-y>
- Mandal, B. B., Grinberg, A., Gil, E. S., Panilaitis, B., Kaplan, D. L., High-strength silk protein scaffolds for bone repair, *P. Natl. Acad. Sci. USA* **109** (2012) 7699. doi: <https://doi.org/10.1073/pnas.1119474109>
- Mottaghtalab, F., Hosseinkhani, H., Shokrgozar, M. A., Mao, C., Yang, M., Farokhi, M., Silk as a potential candidate for bone tissue engineering, *J. Control. Release* **215** (2015) 112. doi: <https://doi.org/10.1016/j.jconrel.2015.07.031>
- Keihan, R. E., Chenab, K. K., Ledari, R. T., Mosafar, J., Hashemi, S. M., Mokhtarzadeh, A., Maleki, A., Hamblin, M. R., Recent advances in the application of mesoporous silica-based nanomaterials for bone tissue engineering, *Mat. Sci. Eng. C* **107** (2020) 110. doi: <https://doi.org/10.1016/j.msec.2019.110267>
- Khan, R. E., Maleki, A., Guardia, M., Bani, M. S., Chenab, K. K., Panahi, P. P., Baradaran, B., Mokhtarzadeh, A., Hamblin, M. R., Carbon based nanomaterials for tissue engineering of bone: Building new bone on small black scaffolds, A review, *J. Adv. Res.* **18** (2019) 185. doi: <https://doi.org/10.1016/j.jare.2019.03.011>
- Melke, J., Midha, S., Ghosh, S., Ito, K., Hofmann, S., Silk fibroin as biomaterial for bone tissue engineering, *Acta Biomater.* **31** (2016) 1. doi: <https://doi.org/10.1016/j.actbio.2015.09.005>
- Boukamp, P., Petrussevska, R. T., Breitkreutz, D., Hornung, J., Markham, A., Fusenig, N. E., Normal keratinization in a spontaneously immortalized aneuploid human keratinocyte cell line, *J. Cell Biol.* **106** (1988) 761. doi: <https://doi.org/10.1083/jcb.106.3.761>

21. Deyrieux, A. F., Wilson, V. G., In vitro culture conditions to study keratinocyte differentiation using the HaCaT cell line, *Cytotechnology* **54** (2007) 77.
doi: <https://doi.org/10.1007/s10616-007-9076-1>
22. Zdraveva, E., Mijović, B., Grgurić, T. H., Govorčin Bajsić, E., Dekaris, I., Trcin, M. T., Ujčić, M., Kaziur, P., Maslanka, P., The effect of the filler and layers on the properties of electrospun antibiotic/fibroin scaffolds, in Novak, I. et al. (Eds.), *The Book of Proceedings of the 12th International Scientific – Professional Symposium Textile Science & Economy French – Croatian Forum*, University of Zagreb Faculty of Textile Technology, Croatia, 2019, pp. 142-149.
23. Tsuji, H., Ishizaka, T., Porous Biodegradable Polyesters, 3. Preparation of porous poly (ϵ -caprolactone) films from blends by selective enzymatic removal of poly (L-lactide), *Macromol. Biosci.* **1** (2001) 59.
doi: [https://doi.org/10.1002/1616-5195\(20010301\)1:23.0.CO;2-6](https://doi.org/10.1002/1616-5195(20010301)1:23.0.CO;2-6)
24. Slivac, I., Zdraveva, E., Ivančić, F., Žunar, B., Holjevac Grgurić, T., Gaurina Srček, V., Svetec, I. K., Dolenc, T., Govorčin Bajsić, E., Tominac Trcin, M., Mijović, B., Bioactivity comparison of electrospun PCL mats and liver extracellular matrix as scaffolds for HepG2 cells, *Polymers* **13** (2021) 279.
doi: <https://doi.org/10.3390/polym13020279>
25. Deitzel, J. M., Kleinmeyer, J., Harris, D., Tan, N. B., The effect of processing variables on the morphology of electrospun nanofibers and textiles, *Polymer* **42** (2001) 261.
doi: [https://doi.org/10.1016/S0032-3861\(00\)00250-0](https://doi.org/10.1016/S0032-3861(00)00250-0)
26. Wei, M., Kang, B., Sung, C., Mead, J., Core-sheath structure in electrospun nanofibers from polymer blends, *Macromol. Mater. Eng.* **291** (2006) 1307.
doi: <https://doi.org/10.1002/mame.200600284>
27. Jin, H. J., Kaplan, D. L., Mechanism of silk processing in insects and spiders, *Nature* **424** (2003) 1057.
doi: <https://doi.org/10.1038/nature01809>
28. Zhou, S., Deng, X., Yang, H., Biodegradable poly (ϵ -caprolactone)-poly (ethylene glycol) block copolymers: Characterization and their use as drug carriers for a controlled delivery system, *Biomaterials* **24** (2003) 3563.
doi: [https://doi.org/10.1016/s0142-9612\(03\)00207-2](https://doi.org/10.1016/s0142-9612(03)00207-2)
29. Coleman, M., Zarian, J., Fourier-transform infrared studies of polymer blends. II. Poly (ϵ -caprolactone)-poly (vinyl chloride) system, *J. Polym. Sci. Polym. Phys. Ed.* **17** (1979) 837.
doi: <https://doi.org/10.1002/pol.1979.180170509>
30. Maddaiah, M., Kumar, A. G. S., Obulapathi, L., Sarmash, T. S., Naidu, K. C. B., Rani, D. J., Rao, T. S., Synthesis and characterization of strontium doped zinc manganese titanate ceramics, *Dig. J. Nanomater. Bios.* **10** (2015) 155.
doi: <https://doi.org/10.1080/17458080.2015.1025302>
31. Lu, Q., Hu, X., Wang, X., Kluge, J. A., Lu, S., Cebe, P., Kaplan, D. L., Water-insoluble silk films with silk I structure, *Acta Biomater.* **6** (2010) 1380.
doi: <https://doi.org/10.1016/j.actbio.2009.10.041>
32. Yang, H., Yang, S., Kong, J., Dong, A., Yu, S., Obtaining information about protein secondary structures in aqueous solution using Fourier transform IR spectroscopy, *Nat. Protoc.* **10** (2015) 382.
doi: <https://doi.org/10.1038/nprot.2015.024>
33. Ha, S. W., Tonelli, A. E., Hudson, S. M., Structural studies of bombyx mori silk fibroin during regeneration from solutions and wet fiber spinning, *Biomacromolecules* **6** (2005) 1722.
doi: <https://doi.org/10.1021/bm050010y>
34. Lu, Q., Zhang, B., Li, M., Zuo, B., Kaplan, D. L., Huang, Y., Zhu, H., Degradation mechanism and control of silk fibroin, *Biomacromolecules* **12** (2011) 1080.
doi: <https://doi.org/10.1021/bm101422j>
35. Elzein, T., Nasser-Eddine, M., Delaite, C., Bistac, S., Dumas, P., FTIR study of polycaprolactone chain organization at interfaces, *J. Colloid Interface Sci.* **273** (2004) 381.
doi: <https://doi.org/10.1016/j.jcis.2004.02.001>
36. Amornsudthiwat, P., Mongkolnavin, R., Kanokpanont, S., Improvement of early cell adhesion on Thai silk fibroin surface by low energy plasma, *Coll Surface B*, **111** (2013) 579.
doi: <https://doi.org/10.1016/j.colsurfb.2013.07.009>
37. Lim, C., Tan, E., Ng, S., Effects of crystalline morphology on the tensile properties of electrospun polymer nanofibers, *Appl. Phys. Lett.* **92** (2008) 141908.
doi: <https://doi.org/10.1063/1.2857478>
38. Magoshi, J., Nakamura, S., Studies on physical properties and structure of silk. Glass transition and crystallization of silk fibroin, *J. Appl. Polym. Sci.* **19** (1975) 1013.
doi: <https://doi.org/10.1002/app.1975.070190410>
39. Bai, L., Li, Q., Duo, X., Hao, X., Zhang, W., Shi, C., Feng, Y., Electrospun PCL-PIBMD/SF blend scaffolds with plasmid complexes for endothelial cell proliferation, *RSC Advances* **7** (2017) 39452.
doi: <https://doi.org/10.1039/C7RA06253B>
40. Ho, M. P., Wang, H., Lau, K.-T., Thermal properties and structure conformation on silkworm silk fibre, in *Proceedings of the Composites Australia and CRC-ACS Conference (CRCACS 2012) Composites Australia, Australia, 2012*, pp. 1-8.
41. Chen, J. P., Chang, Y. S., Preparation and characterization of composite nanofibers of polycaprolactone and nanohydroxyapatite for osteogenic differentiation of mesenchymal stem cells, *Colloid. Surf. B Biointerfaces* **86** (2011) 169.
doi: <https://doi.org/10.1016/j.colsurfb.2011.03.038>
42. Gargotti, M., Efeoglu, E., Byrne, H. J., Casey, A., Raman spectroscopy detects biochemical changes due to different cell culture environments in live cells in vitro, *Anal. Bioanal. Chem.* **410** (2018) 7537.
doi: <https://doi.org/10.1007/s00216-018-1371-5>
43. Luetchford, K. A., Chaudhuri, J. B., De Bank, P. A., Silk fibroin/gelatin microcarriers as scaffolds for bone tissue engineering, *Mater. Sci. Eng. C-Mater.* **106** (2020) 110.
doi: <https://doi.org/10.1016/j.msec.2019.110116>
44. Sun, W., Zhang, Y., Gregory, D. A., Jimenez-Franco, A., Tomeh, M. A., Lv, S., Wang, J., Haycock, J. W., Lu, J. R., Zhao, X., Patterning the neuronal cells via inkjet printing of self-assembled peptides on silk scaffolds, *Prog. Nat. Sci. Mater. Int.* **30** (2020) 686.
doi: <https://doi.org/10.1016/j.pnsc.2020.09.007>